

Unsupervised Reaction Pathways Search for the Oxidation of Hypergolic Ionic Liquids: 1-Ethyl-3-methylimidazolium Cyanoborohydride (EMIM⁺/CBH⁻) as a Case Study

Published as part of *The Journal of Physical Chemistry virtual special issue "Honoring Michael R. Berman"*.

Kazuumi Fujioka, Ralf I. Kaiser, and Rui Sun*



Cite This: *J. Phys. Chem. A* 2023, 127, 913–923



Read Online

ACCESS |



Metrics & More

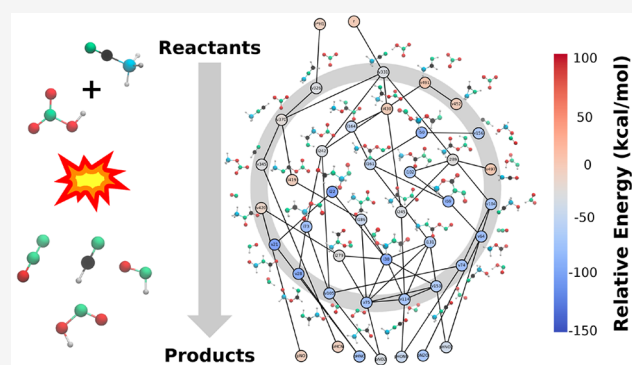


Article Recommendations



Supporting Information

ABSTRACT: Hypergolic ionic liquids have come under increased study for having several desirable properties as a fuel source. One particular ionic liquid, 1-ethyl-3-methylimidazolium/cyanoborohydride (EMIM⁺/CBH⁻), and oxidant, nitric acid (HNO₃), has been reported to be hypergolic experimentally, but its mechanism is not well-understood at a mechanistic level. In this computational study, the reaction is first probed with *ab initio* molecular dynamics simulations to confirm that anion–oxidant interactions likely are the first step in the mechanism. Second, the potential energy surface of the anion–oxidant system is studied with an in-depth search over possible isomerizations, and a network of possible intermediates are found. The critical point search is unsupervised and thus has the potential of identifying structures that deviate from chemical intuition. Molecular graphs are employed for analyzing 3000+ intermediates found, and nudged elastic band calculations are employed to identify transition states between them. Finally, the reactivity of the system is discussed through examination of minimal energy paths connecting the reactant to various common products from hypergolic ionic liquid oxidation. Eight products are reported for this system: NO, N₂O, NO₂, HNO, HONO, HNO₂, HCN, and H₂O. All reaction paths leading to these exothermic products have overall reaction barriers of 6–7 kcal/mol.



I. INTRODUCTION

Hypergolic bipropellants are combinations of a fuel and an oxidizer that spontaneously ignite upon contacting with each other.¹ Compared to normal, nonhypergolic fuels, hypergolic bipropellants do not require an external ignition source thus reducing the design and mass of the engine, which is ideal for space vehicles such as satellites and rockets.² Traditionally, hypergolic bipropellants have employed hydrazine (H₂NNH₂), monomethyl hydrazine (MMH, CH₃(NH)NH₂), and unsymmetrical dimethyl hydrazine (UDMH, H₂NN(CH₃)₂) as the fuel and dinitrogen tetroxide (NTO, N₂O₄) as the oxidizer.^{3–5} In addition to the hypergolicity, the combination of these molecules also features desirable characteristics such as high energy density, low viscosity, short ignition delay, and low-cost synthesis.^{6–8} However, there are serious environmental concerns regarding these chemicals: hydrazine and its derivatives are highly toxic and carcinogenic, while NTO is toxic, corrosive, and highly volatile.^{9,10} Therefore, environmentally friendly, high-performance alternative hypergolic bipropellants are greatly desired.

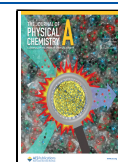
Schneider et al.¹¹ reported the first hypergolic ionic liquid (HIL) in 2008: an imidazolium-based cation coupled with

dicyanamide anion as the fuel (Scheme 1) and red fuming nitric acid (RFNA, ~83% HNO₃ plus 14% N₂O₄ plus ~2% H₂O plus 0.6% HF) or white fuming nitric acid (WFNA, ~100% HNO₃) as the oxidizers. These HILs feature low melting point; viscosity; thermal, impact, and friction sensitivity; and vapor pressure and have inspired extensive research to further develop HIL as a fuel.¹² Currently, there are a considerable number of molecules (e.g., imidazolium-based,¹³ triazolium-based,¹⁴ and tetrazolium-based¹⁵ salts as the cation; dicyanamide and nitrocyamide as the anion) (Scheme 1) categorized as HILs that can be coupled with various oxidizers (IRFNA and WFNA) and rocket-grade hydrogen peroxide (RGHP, H₂O₂ > 90%). The physicochemical properties such as glass transition temperature, melting point, thermal decomposition temperature, density, heat of formation, detonation velocity and pressure, impact and friction

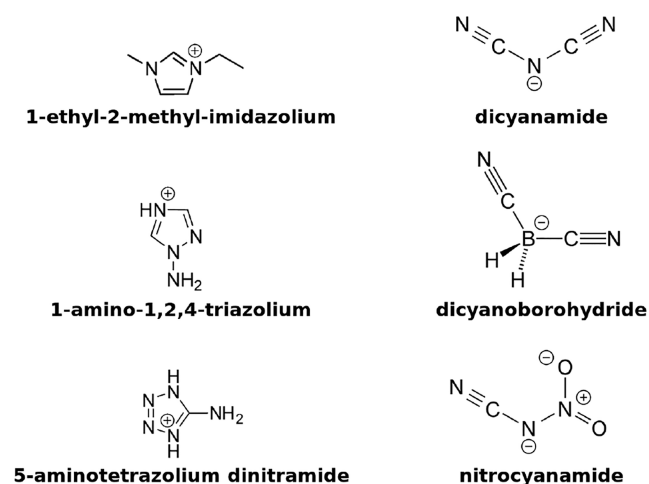
Received: October 31, 2022

Revised: December 9, 2022

Published: December 27, 2022



Scheme 1. Examples of Hypergolic Ionic Liquids



sensitivity, and ignition delay of the HILs are essential to their application as hypergolic bipropellants. Very often, the ID, which is ideally less than 50 μ s, is the most severe limiting factor.⁶ ID has been attributed to a physical delay, e.g., the time that it takes the IL and oxidizer to adequately mix, and a chemical delay, e.g., the time that it takes for the initial reaction after mixture. Although there has been a general consensus that the anion is largely responsible for the chemical properties of HILs and that the cation determines their physical properties,¹⁶ a recent computational study reports that the potential energy profile of the HIL-oxidation reaction changes significantly in the presence of different cations.¹⁷

An elucidation of the mechanism of the ID requires a thorough understanding of the nature of the hypergolicity of HILs, which unfortunately remains elusive at the current stage. This is largely due to the challenges involved in probing the highly energetic, reactive, and transient species in the initial stage of the ignition process *in situ*. Computational studies have proposed that a proton transfer from nitric acid to the anion is the trigger of the hypergolic reaction,^{18–20} whose overall barriers have been claimed to decrease with additional oxidizer;²¹ however, the reported overall reaction barriers are usually too high in energy, e.g., tens of kcal/mol above the reactants, thus seeming to contradict the experimental result—automatic, fast ignition upon the contact between HIL and oxidizer at room temperature. In fact, *ab initio* molecular dynamics (AIMD) simulations of the bimolecular collision between the anion of the HIL and the oxidizer have been carried out at elevated energies of a few thousand Kelvin and/or tens of kcal/mol of collision energy in order to collect a meaningful number of reactive trajectories within a reasonable amount of simulation time.^{18–20} While AIMD is an invaluable tool to find novel, energetically accessible geometries, it alone is simply inadequate to explore these low-reactivity systems at experimental conditions.

One challenge in characterizing the potential energy profile of the oxidation of HIL is the system's complexity. Traditionally, the reaction pathways have largely been identified following chemical intuition—by analyzing the structures of the separated reactants, one makes guesses of the structures of the intermediates (e.g., via addition or insertion mechanism) and proposes possible isomerizations that lead those intermediates to products reported by experiment. This method has seen great successes in *validating* reaction mechanisms, e.g., the Walden inversion in the S_N2 reaction^{22,23} and the nitro-to-nitrite shift

before forming NO.^{24,25} In other words, the reaction pathways found with quantum chemistry calculations confirm the mechanisms that one hypothesizes to take place. When it comes to *exploring* a new reaction pathway that is out of the realm of chemical intuition, this method certainly bares its shortcomings—one could be satisfied once the intuitive pathways are identified and prematurely stop further searching. One such example is the S_N2 reaction (e.g., $F^- + CH_3I \rightarrow CH_3F + I^-$)—the potential energy profiles until around 2008 only were concerned about the traditional Walden inversion pathway with C_{3v} symmetry, and chemists did not start looking for another pathway until guided-beam experiments and AIMD simulations revealed a uniform scattering angle distribution at low collision energy instead of the traditionally believed forward scattering.²⁶ The counterintuitive experimental and AIMD results inspired chemists to search a much larger geometrical space, and as a result, various new pathways (e.g., the hydrogen bond pathway) were discovered.²⁷

Therefore, for the HIL/oxidizer system, it begs the question of whether there exist counterintuitive reaction pathways that have been hidden from potential energy profile searches guided by chemical intuition. In this paper, cyanoborohydride-based HILs [e.g., EMIM⁺ (1-ethyl-3-methylimidazolium, cation)/CBH⁻ (cyanoborohydride, anion), Figure 1] are employed as the

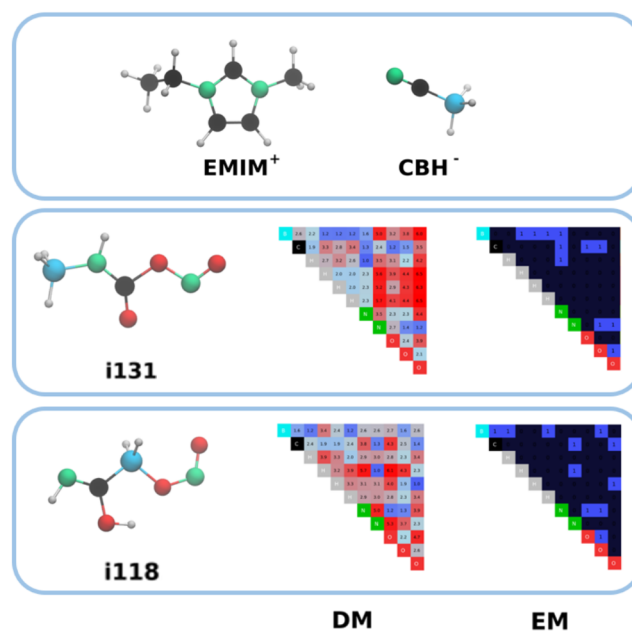


Figure 1. (top) Molecular structure of EMIM⁺ and CBH⁻. (middle and bottom) Examples of two intermediates and their distance matrix (DM) and edge-adjacency matrix (EM). The unit of elements in DM is Å and is represented as the distance for clarity. It should be noted that DM is processed with inverse distances as noted in eq 1.

example system to explore the answer due to the simple chemical structure of the anion. EMIM⁺/CBH⁻ was first reported to be hypergolic upon contacting with HNO₃ as the oxidizer in 2011.²⁸ Even if one assumes only the anion (CBH⁻) and the oxidizer (HNO₃) to be responsible for the initial ignition and consecutive reactions, there are still 11 atoms in the system. The connections between atoms in a molecule can be represented as edges on a graph (Figure 1), where a pair of bonded atoms result in 1 and a pair of nonbonded atoms results in 0. According to the online encyclopedia of integer

sequences,²⁹ 11 (CBH⁻ and HNO₃ have 11 atoms) *indistinguishable* particles result in 1 018 997 864 distinct graphs. Even if one only considers the case where all atoms are connected (i.e., intermediates), there are still 11 716 571 distinct graphs. For a chemical system like the current one, as least some of the particles are *distinguishable* (e.g., carbon atom and hydrogen atom are distinguishable), making the number of distinct graphs even larger. Clearly, trials of geometry optimizations of such quantity are out of the realm of possibility for computational chemistry at this moment, and molecular graphs of unphysical features (e.g., any hydrogen atom having more than one connection) are not worthy of pursuing. Therefore, certain protocols should be implemented to reduce the number of molecular graphs. Taking CBH⁻ and HNO₃ as an example system, this paper reports such an attempt in solving the mystery around the hypergolicity of HILs.

II. METHODS

II.a. Molecular Representation. In order to find reaction pathways in a hyperdimensional geometrical space, a large number of optimal molecular geometries need to be identified, sorted through, and categorized. Herein two molecular representations are adopted to assist these processes. A molecule's geometry can be encoded as a distance matrix (DM)—an N by N symmetric matrix, where N is the number of atoms, whose elements are

$$DM_{i,j} = \begin{cases} 0 & \text{if } i = j \\ 1/r_{i,j} & \text{if } i \neq j \end{cases} \quad (1)$$

i and j are the indexes of a pair of atoms, and $r_{i,j}$ is the distance between them. DM is invariant to rotation and translation and thus is an ideal molecular representation in dealing with a large number of molecular configurations. The distance matrix deviation (DMD) between two configurations is defined as the norm of the difference between their corresponding DMs, minimized over all possible permutations of indistinguishable atoms (e.g., for the system of CBH⁻ + HNO₃, there are (1!)(1!)(4!)(2!)(3!) = 288 permutations). DMD is used to determine whether two configurations are identical, in which case their DMD should be zero (although a value of 0.001 Å⁻¹ is used in this research due to numerical precision). DMs can be further processed to edge-adjacency matrices (EMs), whose elements are

$$EM_{i,j} = \begin{cases} 0 & \text{if } r_{i,j} > r_{\text{cut}} \\ 1 & \text{if } r_{i,j} \leq r_{\text{cut}} \end{cases} \quad (2)$$

i , j , and $r_{i,j}$ take the previous definition while $r_{\text{cut}} = 2.20$ Å is an empirical distance set to detect whether there exists (i.e., $EM_{i,j} = 1$) a chemical bond between a pair of atoms, with the exception of hydrogen which is restricted to having at most one bond. The edge-adjacency matrix deviation (EMD) is defined in the same way as DMD to determine whether two configurations have the same connectivity. In this way, molecules of the same distinct graph (EMD = 0, those with the same connectivity between atoms) may be grouped first, and different conformers (DMD > 0.001 Å⁻¹) will be distinguished among them. An example of DM and EM for a given molecule is shown in Figure 1.

II.b. Initial Geometries. Geometry optimization, following the descent of potential energy of the system, is a local minimization, so it is heavily dependent on the initial

geometries. Each initial geometry is associated with a molecular graph—the number of distinct molecular graphs dictates the number of geometry optimization attempts. To narrow it down, rules used to define valid Lewis structures (enforced by formal charges on carbon, oxygen, nitrogen, and boron atoms) are checked against all possible molecular graphs. SURGE,³⁰ a software which enumerates over all valid Lewis structures given a molecular formula, is used for this procedure, and the result is shown in the Supporting Information. Since there are still 24 183 distinct molecular graphs with valid Lewis structures, and each molecular graph could lead to multiple optimal structures (e.g., *cis*- vs *trans*- and (*S*)- vs (*R*)-), exhausting this list would be inefficient, and additional arguments should be made to guide the search of reaction pathways.

The first argument is to identify distinct molecular graphs from the association of separated species. These species could be separated reactants or products, which are randomly oriented and set apart by different distances. The system is allowed to evolve following the energy gradient, mostly likely leading to the association between these species and formation of intermediates. The molecular graphs corresponding to those intermediates are good candidates for initial geometries to optimize, as they potentially represent the first (in the case of reactants) or the last (in the case of products) step of the chemical reaction. It is important to note that, for reactants, various isomers of CBH⁻ and proton transfer species (e.g., NO₃⁻ and HCBH) are considered, while for the products, they are generated by considering common gas phase products (e.g., NO, NO₂, H₂O, HCN, etc.) of cyanoborohydride-based HIL oxidation plus the remaining molecules. The second argument is to identify distinct molecular graphs from AIMD trajectories of bimolecular collisions of the reactants. The EMs of each frame of the AIMD trajectories are calculated and tallied, and those highly populated EMs are used as initial geometries to optimize. These geometries are ideal candidates for intermediates as their high population in the trajectories signifies a low free energy. These two arguments carry little to no chemical intuition in generating initial geometries and have been reported to identify reaction pathways that are less obvious. These two arguments focus on different geometrical spaces of the system and rely on little to no chemical intuition. The last argument, but certainly not the least, is to be inspired by literature of cyanoborohydride-based HIL oxidation and to draw molecular graphs following similar reaction mechanisms.

II.c. Computation Details. NWChem³¹ is employed for characterizing the reactants, products, intermediates, and transition states. Geometry optimizations and frequency calculations are carried out with B3LYP/6-31G* level of theory,^{32,33} which has been reported to have a good balance between computation cost and accuracy to model cyanoborohydride-based HIL oxidations.¹⁹ The intermediates are confirmed by the number of frequencies ($3N - 6$, $N = 11$, the number of atoms in the system). Between any two intermediates, for the transition state search, the initial geometries are first obtained by interpolation of the intermediates' geometries and, if failed, obtained by nudged elastic band (NEB) calculation.³⁴ In the NEB method, changes in a molecule's geometry are taken step-by-step over a path, and the path is manipulated like an elastic band to minimize the energy traversed over the path. When the path is nudged in a specific way, it converges to the minimal energy path (MEP). The highest energy point of the MEP is then necessarily the saddle point (transition state) between the two end points of the

path: in this case, two local minima (intermediates). The transition states are also confirmed by the number of frequencies ($3N - 7$ and exactly one imaginary frequency). Finally, connections between a transition state and intermediates are confirmed by intrinsic reaction coordinate (IRC)³⁵ calculations with the Gonzalez–Schlegel algorithm.³⁶ The connections between separated species (reactants or products) and intermediates are confirmed by the direct association of these species.

AIMD simulations are carried out with VENUS/NWChem.³⁷ Energy and force calculations are carried out with the same B3LYP/6-31G* level of theory with a time step of 0.5 fs. For bimolecular collisions, the reactants are separated by 8 Å with an impact parameter of 0 Å. The vibrational and rotational energy are sampled from a canonical ensemble of 300 K, while their collision energy is 11 kcal/mol. For unimolecular dissociations, the vibrational and rotational energy of the reactants are sampled from a canonical ensemble of 3000 K. Trajectories are stopped if the molecules have been separated by more than 6 Å after collision.

III. RESULTS AND DISCUSSION

III.a. AIMD Simulations. Table 1 lists the initial species of various AIMD simulations of bimolecular collisions and their

Table 1. Summary of the AIMD Simulations' Bimolecular Collisions^a

colliding species		N_T	N_R	products
CBH ⁻	HNO ₃	50	1	HCBH + NO ₃ ⁻
EMIM ⁺	HCBH	40	5	EMIM ⁺ + BH ₃ + HNC
			10	EMIM ⁺ + H ₂ BCHNH (r^*_{H4})
			2	EMIM ⁺ + <i>c</i> -H ₂ BCHNH (r^*_{H2})
EMIM ⁺ /HCBH	NO ₃ ⁻	30	4	EMIM ⁺ /CBH ⁻ (<i>r</i>) + HNO ₃
EMIM ⁺ /NO ₃ ⁻	HCBH	60	14	EMIM ⁺ /HNO ₃ + CBH ⁻ (<i>r</i>)
			1	EMIM/HNO ₃ + HCBH

^a N_T is the total number of trajectories. N_R is number of reactive trajectories. The structures of each species can be found in Figure 2.

products. It is important to reemphasize that these AIMD trajectories are not intended to mimic the experimental conditions of the HIL oxidation because the collision energy in the simulations would be too high, but instead, they are simply to explore the geometrical space of the reaction without chemical intuition (section II.b). Even though the number of trajectories simulated is comparable to previous AIMD studies,^{38,39} the complexity of the PES will necessitate further exploration in section III.b. As noted in the Introduction, proton transfer from HNO₃ to the anion has been proposed as the first step of the cyanoborohydride-based HIL oxidation reaction. Therefore, the first set of bimolecular collisions is chosen as HNO₃ colliding with CBH⁻. The proton has been observed to transfer back and forth between HNO₃ and CBH⁻ in 1 out of 50 trajectories; the remaining 49 trajectories are nonreactive. Nonetheless, this result indicates that NO₃⁻ and HCBH could also be participating in this reaction.

The second set of biomolecular collisions between EMIM⁺ and HCBH is carried out, and the trajectories are more reactive. About 10% of the trajectories observe the scission of the boron–carbon bond and the formation of BH₃ + HNC. Another 30% of the trajectories observe isomerization of HCBH after it collides with EMIM⁺, during which the hydrogen in the –BH₃ group migrates to carbon, resulting in H₂BCHNH or its cyclic isomer,

c-H₂BCHNH (r^*_{H4} and r^*_{H2} , respectively, Figure 2). Two more sets of AIMD simulations mimicking the consecutive bimolecular collisions after the initial proton transfer between the oxidizer and anion (i.e., HNO₃ + CBH⁻ → NO₃⁻ + HCBH) are carried out: (1) between EMIM⁺/HCBH and NO₃⁻, about 90% of the collisions are nonreactive, and the proton transfers from HCBH back to NO₃⁻ in the remaining 10%, and (2) between EMIM⁺/NO₃⁻ and HCBH, about 75% of the collisions are nonreactive, and the proton transfers from HCBH back to NO₃⁻ in the remaining 25%. In the second case, one trajectory observes the transfer of a proton from the C2 carbon of the imidazolium of EMIM⁺ to NO₃⁻, resulting in EMIM/HNO₃. These simulations together show that although the presence of EMIM⁺ increases the reactivity by about 10-fold, the anion and the oxidizer are still the centerpiece of the initial step of the hypergolic reaction of HIL—all except one trajectory sees involvement of EMIM⁺ in the chemical reaction. Therefore, the focus will be on the anion (CBH⁻) and the oxidizer (HNO₃) for the rest of the paper.

Focusing on the anion and oxidant, exploration with AIMD may continue by starting with an anion–oxidant intermediate and simulating a thermal excitation. Unfortunately, no intermediate with significant lifetime is observed in the bimolecular collision trajectories; e.g., molecules fly apart from each other immediately after collision for both reactive and nonreactive trajectories. Therefore, unimolecular dissociations starting from six different intermediates (Table 2) are carried out with AIMD simulations. Compared to bimolecular collisions, unimolecular dissociation guarantees reactions (given enough simulation time and excess energy) and thus has the potential of being more effective in detecting reaction pathways. These intermediates for dynamics simulations (IDS) either have been reported by previous research³⁹ (e.g., IDS1, the hydrogen bond complex between HNO₃ and CBH⁻; IDS2, NO₃⁻ attached to the carbon atom on HCBH; IDS3, migration of the –NO₂ from oxygen to nitrogen in IDS2; and IDS4, NO₃⁻ attached to the boron atom of an isomer of HCBH) or are proposed according to chemical intuition (e.g., ISD5, migration of the –NO₂ from oxygen to carbon in IDS2; ISD6, migration of the –BH₃ from carbon to oxygen and the transition from nitro to nitrite in IDS5). It is important to note that this list is by no means exhaustive—the trajectories initiated from IDSs of different bond connections sample diverse chemical configurations and aim to detect potential products which will be employed to search for intermediates (section II.b). While a larger number of trajectories may eventually elucidate a more complete picture of all of the intermediates and pathways, the existing results necessitate continued searching. The results of these unimolecular dissociation AIMD simulations are summarized in Table 2. As shown, with an excessive amount of thermal energy (e.g., 3000 K), almost all intermediates have dissociated. The identities of the products heavily depend on the initial geometry of the unimolecular decomposition. For example, over 60% of IDS1 decomposes to reactants (e.g., HNO₃ + CBH⁻ or NO₃⁻ + HCBH), confirming that IDS1 is an entrance-channel intermediate. BH₃ is the most dominant product overall, which is found in all unimolecular decomposition trajectories, followed by NO₂, which is only not found in the decomposition of ISD1. Other species such as HCN, CO, CO₂, and HN₂O₂ also make a statistically significant contribution to a list of diverse products.

III.b. Critical Point Search. Figure 3a demonstrates a map of the critical points of a distinct molecular graph found

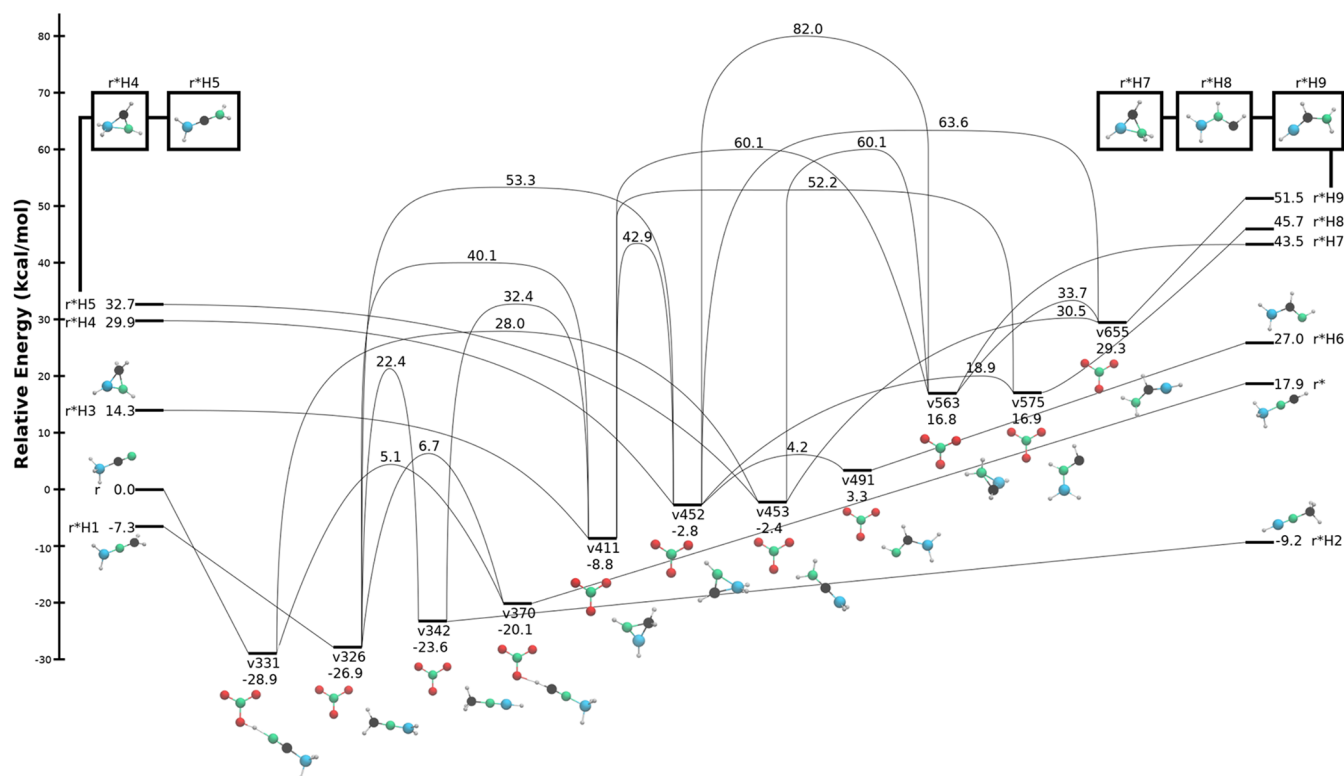
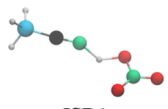

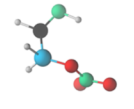



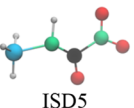
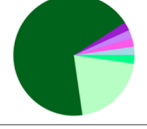
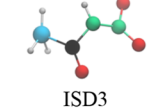
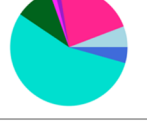

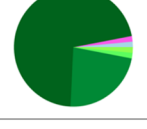


Figure 2. Potential energy profile of the interconversion between various forms of reactants initiated from CHB^- and HNO_3 (r). Zero-point energies are included.

Table 2. Summary of the AIMD Simulations of Unimolecular Dissociation Initiated from Various Intermediates

Initial Species	Results	Initial Species	Results
 ISD1		 ISD4	
 ISD2		 ISD5	
 ISD3		 ISD6	

Legend for Results:

- Nonreactive
- $\text{H}_3\text{BCN} + \text{HNO}_3$
- $\text{H}_3\text{BCNH} + \text{NO}_3$
- $\text{H}_3\text{BCN} + \text{H}_2\text{NO}_3$
- $\text{H}_3\text{BNO}_3 + \text{HCN}$
- $\text{H}_3\text{B} + \text{CO}_2 + \text{HNO}_2$
- $\text{H}_3\text{B} + \text{CN} + \text{HNO}_3$
- $\text{H}_3\text{B} + \text{CO} + \text{HN}_2\text{O}_2$
- $\text{H}_3\text{B} + \text{CNO} + \text{HNO}_2$
- $\text{H}_3\text{B} + \text{HCN} + \text{NO}_3$
- $\text{H}_3\text{B} + \text{HCNO} + \text{NO}_2$
- $\text{H}_3\text{BN}_2\text{O}_2 + \text{CO}$
- $\text{HBO} + \text{H}_3\text{CN} + \text{NO}_2$
- $\text{H}_3\text{BCO} + \text{HN}_2\text{O}_2$
- $\text{H}_3\text{BCO}_2 + \text{HN}_2\text{O}$
- $\text{HBO} + \text{H}_2\text{CN} + \text{HNO}_2$
- $\text{H}_3\text{BCNO} + \text{HNO}_2$
- $\text{H}_3\text{BCNO} + \text{NO}_2$

following the protocol listed in section II.b. As messy as this figure has already been, unfortunately it is still not an exhaustive map of all the 3000+ intermediates found. Instead, each bead on the map is possibly only one representation of a series of intermediates of the same molecular graph. For example, as shown in Figure S1, there are 12 intermediates of the same molecular graph and very similar energies. They are connected by a slight geometrical distortion, and they are represented by only one bead in Figure 3a. Altogether, there are a total of 370 beads depicted in Figure 3a, which are put into two categories—the ones on the circle edges shaded with gray are the van der Waals and hydrogen bond complexes (85, noted with “v”), and the ones inside are regular intermediates (285, noted with “i”).

The relative energies (REs) with respect to the reactants are used to color each bead. If two intermediates are connected by a solid line, it means that they are connected by a transition state confirmed by IRC. If a separated species (reactants or products) is connected to an intermediate, it means the association is barrierless. In addition to CBH^- and HNO_3 , there can be multiple forms of reactants (the example given in the previous section is the proton-transferred reaction, HCBH and NO_3^- , also see Figure 2) involved in this reaction, and more details will be given later in the paper. Overall, all the intermediates together, as shown in the central circle of Figure 3a, act like a “chemistry blender” that turns the reactants on top to the products at the bottom. Instead of analyzing a certain reaction

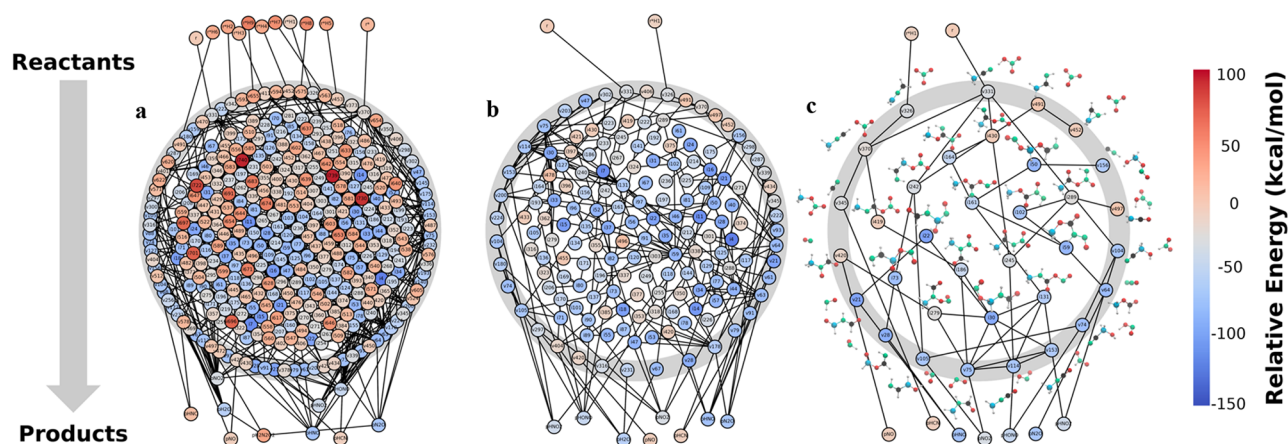


Figure 3. Map of the critical points of distinct molecular graphs connecting the reactants (on top of the circle) to the products (at the bottom of the circle). The color of each bead represents its (ZPE corrected) relative energy with respect to separate CBH^- and HNO_3 . The gray shaded circle covers the intermediates where two molecules are loosely bonded (e.g., van der Waals and hydrogen bond complexes). A zoomed in picture for each subfigure is shown in the [Supporting Information](#).

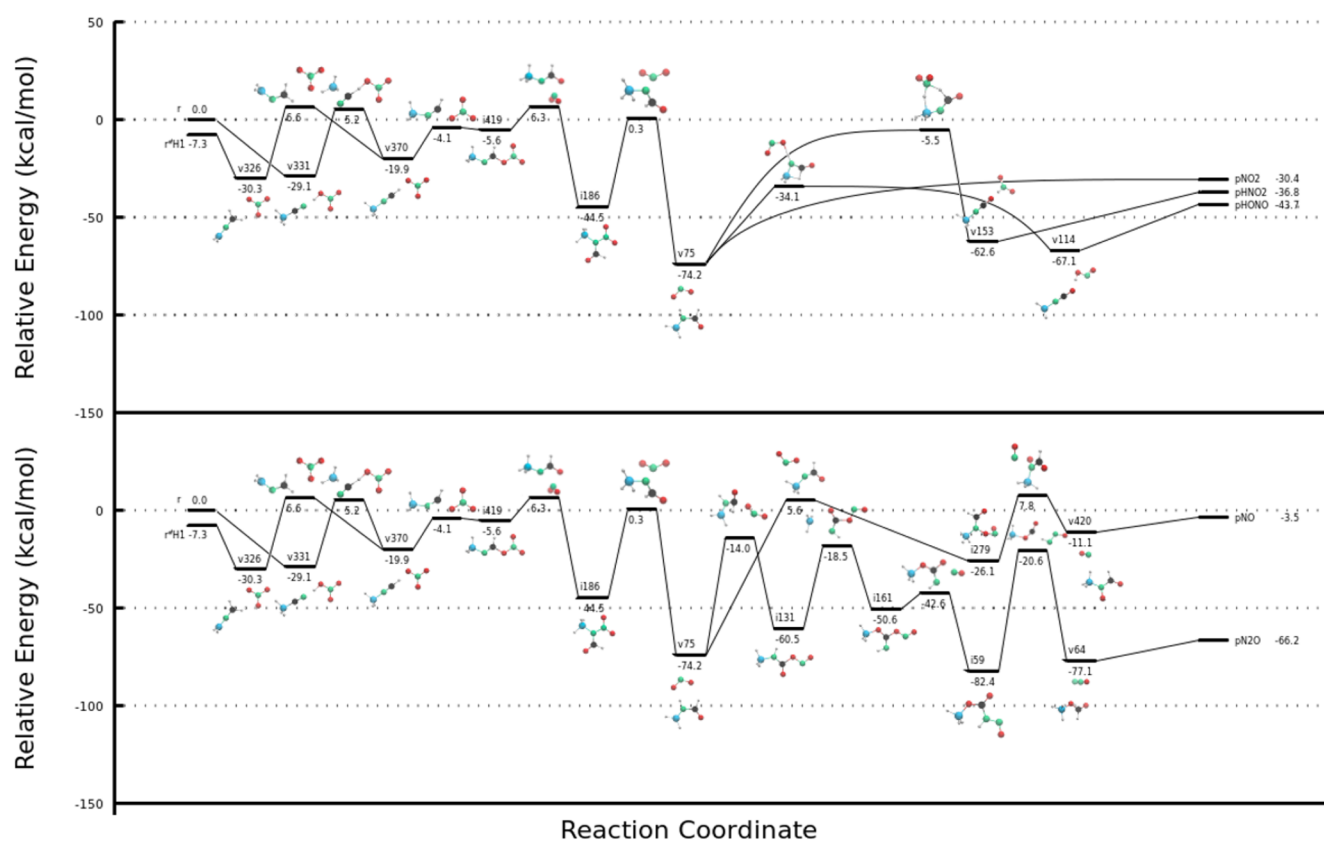


Figure 4. Minimal energy paths of the reactions identified from [Figure 3](#). ZPEs are included.

pathway, [Figure 3a](#) serves as an example to demonstrate the complexity of the oxidation reaction of HILs. It is interesting to note that the reactants are not directly connected to the regular intermediates (inner circle of the map) through addition or insertion, but instead, they go through van der Waals or hydrogen bond complexes first (outer ring of the map). The color of these complexes (changing from exclusively red as reactants to a mixture of red–blue as intermediates and products) suggests that potential energy is released in this process, which can be intuitively understood as restoring kinetic

energy and preparing for further reaction. It is obvious that [Figure 3a](#) contains information that is not relevant to the mechanisms that trigger the initial reaction at room temperature—as there is not enough excess energy to overcome high energy barriers (although the information on the barrier is not shown in this figure). Therefore, an energy cutoff (E_c) is employed to obtain only the relevant information. First of all, the potential energy of the separated reactants (CBH^- and HNO_3) is shifted to zero, and all other species are shifted accordingly. Zero-point energy (ZPE) computed from the frequency of the

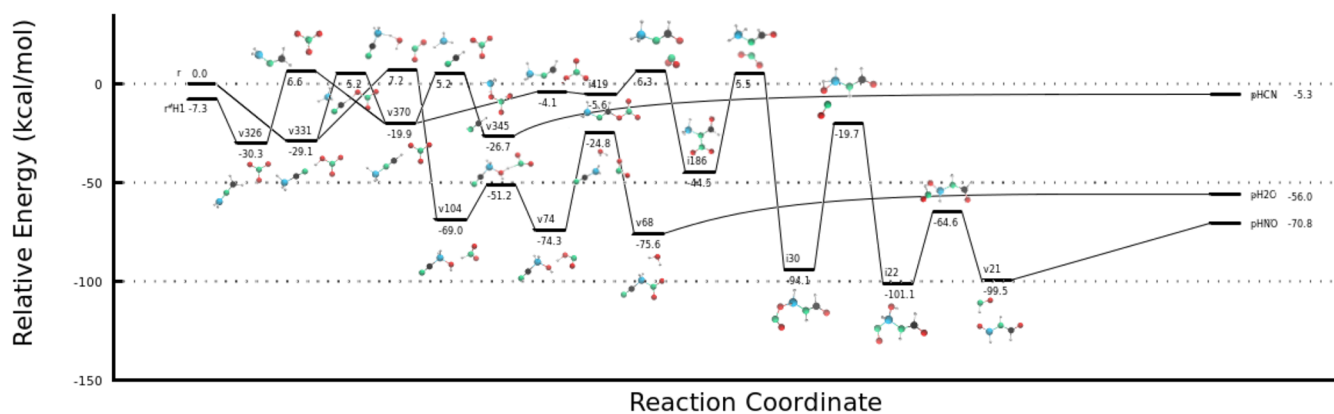


Figure 5. Minimal energy paths of the reactions identified from Figure 3. ZPEs are included.

Table 3. Summary of the Products and Overall Barriers of Each Pathway^a

product	ΔE	E^\ddagger	product	ΔE	E^\ddagger
NO ₂	-30.4	6.3	NO	-3.5	7.8
HONO	-43.7	6.3	HCN	-5.3	5.2
HNO ₂	-36.8	6.3	HNO	-70.8	6.3
N ₂ O	-66.2	6.3	H ₂ O	-56.0	7.2

^a ΔE is the reaction energy, and E^\ddagger is the overall barrier of the pathway. Unit of the energy is kcal/mol. ZPEs are included.

species is included in the energy. In this paper, E_c is chosen as 10 kcal/mol above the potential energy of separated reactants, but in principle, it can be any arbitrary value. Specifically, for separated species (reactants and products), those with a potential energy less than E_c are kept. As shown in Figure 3b, two reactants (the original CBH⁻ and HNO₃, named **r**, as well as a proton-transferred isomer, H₂BNCH₂ and NO₃⁻, named **r***_{H1}) along with eight products (denoted by the identity of the small

gas molecule and starting with “p”) have survived the E_c filtering. A discussion on how they are related will be given later in this paper. For intermediates, those that are connected to at least one transition state less than E_c are kept. The survived intermediates undergo further scrutiny to keep only those that are outwardly connected, which is defined as connecting to at least one product and one reactant through survived intermediates. The reason for enforcing the outward connection is to make sure that the map does not contain a subsection of intermediates that are connected to one another via transition states lower than E_c but are not connected to reactants or products. These intermediates, although possessing valid chemical structures of low energy, are not relevant to the mechanisms that trigger the initial reaction at room temperature.

Figure 3b summarizes the species after the filtering. Although the information in this figure has been significantly reduced, there are still numerous pathways connecting a reactant to a product. Among all the potential pathways, those that overcome a low energy barrier are more likely to be populated compared to

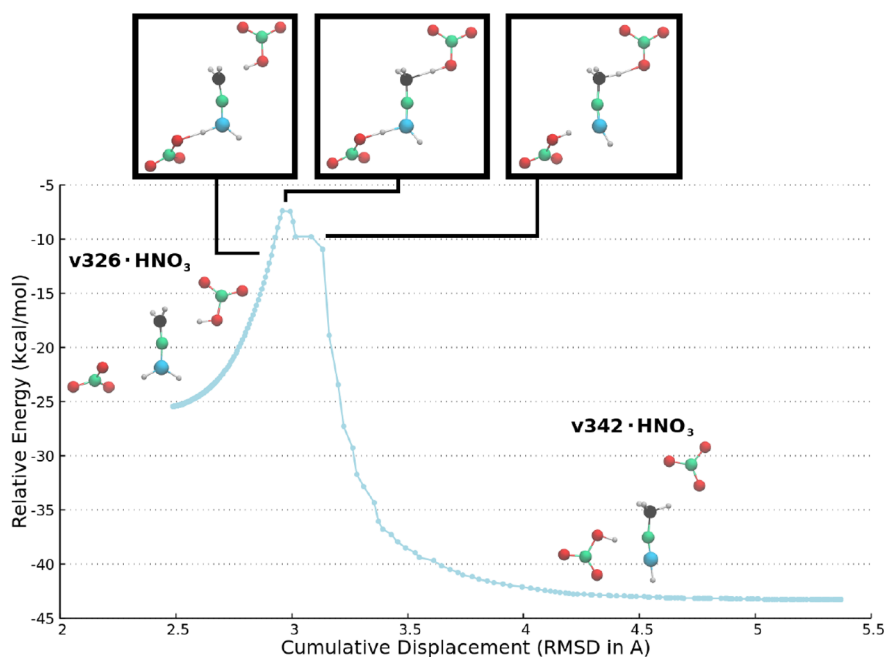


Figure 6. Relative potential energy (with respect to separated trimolecule, HNO₃ + CBH⁻ + HNO₃) with respect to the intrinsic reaction coordinate transiting from v326 to v342. The same process is depicted in Figure 2 for a bimolecular system (CBH⁻ + HNO₃).

the ones associated with a high energy barrier. In order to find the MEP from the reactants to products, Figure 3b is further filtered following three steps: (1) For each pair of reactant and product, all possible pathways are identified. (2) Among all the pathways identified in step one, the pathways possessing the lowest overall barriers (defined as the most significant barrier) are selected. (3) If step two results in multiple pathways, one with the shortest chemical distance (i.e., involving the smallest number of intermediates) is selected as the MEP. This procedure is carried out for all pairs between two reactants and eight products in Figure 3b, and the results are summarized in Figure 3c. Further breakdowns of MEPs identified in Figure 3c are provided later in the paper. Starting from Figure 3a, which contains all chemical information (e.g., reactants, products, intermediates, and transition states) found in unsupervised geometry searches, the procedure presented in this paper first reduces the amount of the information with a tunable energy cutoff (Figure 3b), from which the MEPs for this very complicated reaction system are identified. These MEPs represent the most probable reaction pathways when the excess energy is low and thus can potentially unravel the mechanisms that trigger the hypergolic reaction at room temperature.

III.c. Interconversion of the Reactants. As noted in section III.a, the reactants (r , CBH^- and HNO_3) could undergo a proton transfer process before the oxidation reaction. Other research has also reported that the proton transfer is a key step in the hypergolic reactions of ionic liquids. Herein, we investigate extensively the possible interconversions of the reactants. Figure 2 summarizes the relative energy and structures of 11 different forms of the reactants and various intermediates that facilitate the interconversions. The association between CBH^- and HNO_3 (r) results in $v331$ and releases 28.9 kcal/mol of energy. $v331$ could cross a B–C–N three-membered ring transition state of 5.1 kcal/mol and form $v370$. The dissociation of $v370$ will result in the proton transferred reactant, H_3BNCH and NO_3^- (r^*), which is 17.9 kcal/mol higher in energy than r . Alternatively, the hydrogen in the $-\text{BH}_3$ group in $v370$ could transfer to the carbon atom on the other end of the molecule after overcoming a transition state of 6.7 kcal/mol and form $v326$. The dissociation of $v326$ results in H_2BNCH_2 and NO_3^- ($r^*_{\text{H}_1}$). It is interesting to note that $r^*_{\text{H}_1}$ is 7.3 kcal/mol lower in energy than the original reactant (r) and can be accessed with moderate excess energy (6.7 kcal/mol overall barrier); thus, $r^*_{\text{H}_1}$ could be important in the initial step of the oxidation reaction. Either other forms of reactants are too high in energy (e.g., $r^*_{\text{H}_9}$), or their formation from the original reactant (r) involves transition states that are too high (e.g., $r^*_{\text{H}_2}$ itself is 9.2 kcal/mol lower than r , representing the lowest energy in all forms of reactants, but forming $r^*_{\text{H}_2}$ from r has an overall barrier of 22.4 kcal/mol). Although these forms of reactant could be relevant once the temperature of the system has increased to a certain level as a result of the oxidation reaction, they are not likely to contribute to the initial reaction that makes the system hypergolic. Therefore, the analysis in the rest of the paper only focuses on the reaction pathways initiated from r and $r^*_{\text{H}_1}$.

III.d. Potential Energy Profile of the Reaction. The MEPs of the reaction identified in Figure 3 are depicted in Figures 4 and 5. The potential energy of all species in Figure 4 are relative to the separated reactant, r . Since the focus of this study is the initial reaction that triggers the hypergolic reaction, the geometry search stops after primary dissociation. A small molecule (normally in the gas phase) is formed as a result of the dissociation, which is accompanied by a residual molecule (for

example, the formation of HONO is accompanied by the formation of H_3BNCO^-). We note that although the residual molecule could possess various conformers and/or undergo further decomposition, they are not the focus of this research, and Figure 3 only presents the isomer as the result of a direct dissociation of the intermediate.

Figure 4 demonstrates the MEPs leading to the formation of NO, NO_2 , N_2O , HNO_2 , and HONO. All these products stem from $v370$, a hydrogen bond intermediate that is accessible to both r and $r^*_{\text{H}_1}$ (see section III.c). This intermediate could overcome a submerged transition state (-4.1 kcal/mol), where the NO_3^- group migrates from interacting with hydrogen to interacting with carbon and results in $i419$ ($\text{H}_3\text{BNC}(\text{H})\text{NO}_3^-$). The O– NO_2 bond in $i419$ could break, and the $-\text{NO}_2$ group reattaches to the residual molecule via a N–N bond, forming $i186$ ($\text{H}_3\text{BN}(\text{NO}_2)\text{C}(\text{H})\text{O}^-$). This step crosses a barrier of 6.3 kcal/mol. The newly formed N– NO_2 bond in $i186$ could also break while a hydrogen is transferred from the $-\text{BH}_3$ moiety to the neighboring nitrogen atom. This step overcomes a barrier of only 0.3 kcal/mol, resulting in another hydrogen bond complex, $v75$. Further isomerization/dissociation of $v75$ leads to five different products:

- (1) $v75$ could dissociate without a barrier to NO_2 and $\text{H}_2\text{BN}(\text{H})\text{C}(\text{H})\text{O}^-$ (pNO_2), and the reaction energy of this pathway is -30.4 kcal/mol with an overall barrier of 6.3 kcal/mol (between $i419$ and $i186$).
- (2) For the residual molecule in $v75$, the hydrogen attached to the carbon atom could transfer to $-\text{BH}_2$ while the hydrogen attached to the nitrogen atom transfers to NO_2 , resulting in another hydrogen bond complex, $v114$, which could dissociate without a barrier to HONO and H_3BNCO^- (pHONO , reaction energy of -43.7 kcal/mol). The transition state between $v75$ and $v114$ is submerged (-34.1 kcal/mol), and the overall barrier of this pathway is the same (6.3 kcal/mol) as the pNO_2 pathway.
- (3) Starting similarly to the previous step (e.g., the hydrogen attached to the carbon atom in the residual molecule transfers to $-\text{BH}_2$), but the NO_2 flips and points its nitrogen atom toward the residual molecule. The submerged transition state (-5.5 kcal/mol) features two N–H interactions—one H belongs to the $-\text{BH}_3$ moiety while the other is attached to carbon—and the latter eventually transits to the nitrogen of the NO_2 group, forming $v153$. $v153$ dissociates without a barrier to form HNO_2 and H_3BNCO^- (pHNO_2). The overall barrier and the reaction energy of this pathway are 6.3 kcal/mol (same as 1 and 2) and -36.8 kcal/mol, respectively.
- (4) An oxygen atom in the NO_2 group in $v75$ could reattach to the carbon atom in the residual molecule; in the meantime, the hydrogen atom on the carbon shifts back to the $-\text{BH}_2$ moiety, resulting in $i131$ ($\text{H}_3\text{BN}(\text{H})\text{C}(\text{O})\text{ONO}$). The $-\text{BH}_3$ moiety in $i131$ migrates from the nitrogen to the carbonyl oxygen and forms $i161$ ($\text{H}_3\text{BOC}(\text{NH})\text{ONO}$). The O–NO bond in $i161$ then breaks, and the NO reforms a N–N bond with the residual molecule, leading to $i59$ ($\text{H}_3\text{BOC}(\text{O})\text{N}(\text{H})\text{NO}$). Sequentially, the hydrogen attached to the nitrogen shifts to the carbon while the N–C bond breaks, forming $v64$ before eventually dissociating to N_2O and $\text{H}_3\text{BOC}(\text{H})\text{O}^-$ (pN_2O , reaction energy of -66.2 kcal/mol). The process from $i75$ to pN_2O is submerged, while the overall barrier

from the reactants to pN_2O is 6.3 kcal/mol (same as 1–3).

- (5) An oxygen atom in the NO_2 group in **v75** could reattach to the nitrogen atom in the residual molecule; in the meantime, the hydrogen atom on the nitrogen shifts back to the $-\text{BH}_2$ moiety, resulting in **i279** ($\text{H}_3\text{BN}(\text{ONO})\text{C}(\text{O})\text{H}$). The $\text{ON}-\text{O}$ bond in the nitrite moiety of **i279** ruptures, and the NO could form a hydrogen bond complex (**v420**) before eventually breaking off from the residual molecule ($\text{NO} + \text{H}_3\text{BN}(\text{O})\text{C}(\text{H})\text{O}$, **pNO**). This pathway stands out from the others because neither of the two steps after **v75** is submerged (between **v75** and **i279**, 5.6 kcal/mol; between **i279** and **v420**, 7.8 kcal/mol), with the second step possessing the highest barrier. The reaction energy of this pathway is -3.5 kcal/mol.

Figure 5 demonstrates the MEPs leading to the formation of HCN , H_2O , and HNO , and their mechanisms are detailed below:

- (6) The $\text{B}-\text{C}$ bond in **v370** ruptures, and the $-\text{BH}_3$ group migrates to form a new $\text{B}-\text{O}$ bond with the oxygen atom in NO_3^- (**v345**). In **v345**, the HCN (after $-\text{BH}_3$ breaking off from CBH^-) interacts with the $\text{H}_3\text{BONO}_2^-$ complex via a hydrogen bond. **v345** could dissociate to HCN and $\text{H}_3\text{BONO}_2^-$ (**pHCN**) in a barrierless process. The transition from **v370** to **v345** involves crossing a barrier of 5.2 kcal/mol, same as the barrier between **v331** and **v370**. HCN is a common product formation for similar reactions, like nitric acid with dicyanoamide or dicyanoborohydride.^{39,40} The reaction energy of the **pHCN** pathway is -5.3 kcal/mol.
- (7) The mechanism of the system transiting from **v370** to **i186** has been explained in the previous paragraph. Instead of forming **v75**, which leads to the formation of NO , NO_2 , N_2O , HNO_2 , and HONO (1–5), the $\text{N}-\text{N}$ bond could break, and the $-\text{NO}_2$ moiety moves down the molecule to form an $\text{O}-\text{B}$ bond. This process is accompanied by one of the hydrogens in the $-\text{BH}_3$ moiety transferring to the nitrogen atom, leading to $\text{ONOB}(\text{H}_2)\text{N}(\text{H})\text{C}(\text{H})\text{O}$ (**i30**). The $-\text{NO}$ moiety in the nitrite terminal of the molecule could break off, and the oxygen left will grab a hydrogen from the adjacent $-\text{BH}_2-$ group. The $-\text{NO}$ moiety reforms a $\text{N}-\text{B}$ bond and results in **i22**, where the backbone of the molecule is $\text{OC}(\text{H})-\text{N}(\text{H})\text{B}(\text{H})\text{NO}$ and the boron atom also coordinates with a hydroxyl group ($-\text{OH}$). **i22** is highly stable (-101.1 kcal/mol) and is the lowest-energy intermediate among all the MEPs. The newly formed $\text{N}-\text{B}$ bond can break, and the $-\text{NO}$ moiety takes the hydrogen away from the hydroxyl group, forming another hydrogen bond complex **v21**. **v21** can dissociate without a barrier and form HNO and $\text{OB}(\text{H})\text{N}(\text{H})\text{C}(\text{H})\text{O}$ (**pHNO**). Although this MEP possesses several low-energy intermediates (e.g., **v21**, **i22**, and **i30**), transiting from **v370** to **pHNO** is not entirely submerged (e.g., the highest barrier is between **i419** and **i186**, 6.3 kcal/mol). The reaction energy of the **pHNO** pathway is -70.8 kcal/mol, the most exothermic reaction path among all the pathways found in this research.
- (8) This pathway stems from **v331**, a hydrogen bond complex as a result of direct association between CBH^- and HNO_3 (**r**). The HNO_3 could move to the $-\text{BH}_3$ end of CBH^- and exchange its hydroxyl with one of the hydrogens from $-\text{BH}_3$ to form **v104**. The HNO_2 group in **v104** undergoes

isomerization, where the hydrogen transfers from nitrogen to oxygen (HONO , **v74**). The hydroxyl group of HONO interacts with the hydroxyl group of the residual molecule, leading to a dehydration condensation and forming **v68**, where the water molecule is loosely interacting with the rest of the molecule. **v68** eventually dissociates to H_2O and $\text{NCB}(\text{H}_2)\text{NO}_2^-$ (**pH₂O**). The most significant barrier of the **pH₂O** pathway is the transition between **v331** and **v104** (7.2 kcal/mol), and the reaction energy of this pathway is -56.0 kcal/mol.

The mechanisms seen here in the MEPs have significant overlap with similar ionic liquid (anion)–oxidant reactions in the literature. For example, studies of nitric acid and dicyanamide^{39,41} as well as nitric acid and dicyanoborohydride^{39,40} have both found proton migration, $-\text{ONO}_2$ attachment to the carbon, and $-\text{NO}_2$ migration as key first steps in the reaction. In the current system, all three mechanisms are seen in a number of transition states connecting intermediates. In fact, they are required steps for the MEPs of the formation of products with the NO_2 or NO group. Now, while the reactions studied in the literature have a few similar individual steps and analogous intermediates, they differ in the types of intermediates. In the current reaction, many more van der Waals or hydrogen bond complexes (about 50%) have been found to be important compared to the two aforementioned reactions. While it is not immediately clear how this may affect the reactivity of the current system, the novelty of the species may give insight into potentially unexplored pathways for other hypergolic ionic liquid systems.

III.e. Mechanism of the Hypergolic Reaction: A Hypothesis. This paper presents a protocol of unsupervised critical point search that locates the MEPs for the reaction between CBH^- and HNO_3 . Table 3 summarizes the products and overall barriers of each pathway. Under the condition of low excess energy, a total of eight primary products are found, and the reactions are all exothermic. However, none of the MEPs that lead to the product are completely submerged, and all possess an overall barrier of 5–7 kcal/mol. Albeit not significant, these barriers could result in the ignition delay or even prevent the hypergolic ignition. For example, in a 300 K thermal distribution, only about 0.0032% of molecules have at least 7 kcal/mol kinetic energy. After all, how does the reaction system overcome such barriers at room temperature? Further, if hypergolic ionic liquids were used as propellants in a space vehicle, the operational temperature would be much lower. The answer lies in the association between CBH^- and HNO_3 —as demonstrated in Figures 2–5, this association leads to a loosely bonded hydrogen bond or van der Waals intermediates while releasing potential energy to kinetic energy. Because of the overall barrier, certainly not all the associations between CBH^- and HNO_3 result in the formation of the products; however, those hydrogen bond or van der Waals intermediates will become vibrationally “hot”, resulting in a transient, locally excited region that offers enough excess energy to molecules within, pushes them over the energy barriers, and forms products. Since all the formed products are exothermic, the temperature of the system will keep on increasing, promoting more reactions to take place.

It is also important to acknowledge the limitations of this study and the hypothesis. The hypergolic reaction upon the mixing of $\text{EMIM}^+/\text{CBH}^-$ and HNO_3 is observed in the condensed (i.e., liquid) phase in experiment. Under such

conditions, the association between CBH^- and HNO_3 involves two steps: (1) CBH^- breaking away from the EMIM^+ (against electrostatic interaction) and HNO_3 breaking away from the rest of the HNO_3 molecules (breaking the hydrogen bond network) and (2) the association between the CBH^- and HNO_3 . The second step is exothermic and has been elaborated in the paper, while the first step is absent and is endothermic. Therefore, with both steps combined, the association between CBH^- and HNO_3 should be less exothermic than predicted in the gas phase calculation. However, as has been documented in other cases,^{25,42} the condensed phase environment could also lower the barrier of chemical reactions. Take the transition between **v326** and **v342**, a transition state where a proton is transferred from $-\text{BH}_2$ to $-\text{CH}_2$ (Figure 2), as an example—the transition state is 49.3 and 46.0 kcal/mol above **v326** and **v342**, respectively. The same transition state is much more accessible with just one additional HNO_3 . As shown in Figure 6, the proton transfer is accomplished via the Grothuss mechanism. In comparison, the height of the transition state is vastly decreased to 17.5 and 37.1 kcal/mol above **v326** and **v342**, respectively. Therefore, to fully capture the dynamics and unravel the mystery of hypergolicity, the free energy of the reaction in the condensed phase simulation is required. An accurate evaluation of the free energy requires a set of collective variables that describe the progress of the reaction, which will be selected from the MEPs identified in this paper and pursued in a future work.

As a final note, while the characterization of the anion–oxidant PES primarily aims to give a foundation for further condensed phase study, it can also give insight into gas-phase kinetics. For instance, even with only the stationary points, transition state theory (TST) rate constants may be calculated and used to calculate reaction rates for a canonical ensemble. With these, product branching ratios can be tabulated which can be directly compared to measured gas formation in experiments. Some of these gaseous products may even further react, such as NO , HNO , and NO_2 , which are known to take part in the gas-phase ignition of nitrogen-rich gas mixtures.^{43–45} The results in this study would benefit greatly from further chemical kinetics analysis.

■ ASSOCIATED CONTENT

SI Supporting Information

The Supporting Information is available free of charge at <https://pubs.acs.org/doi/10.1021/acs.jpca.2c07624>.

Example of molecules with the same molecular graph and very similar energies, brief description of the method of computing unique molecular graphs for the current system, and zoomed-in picture of the chemistry map (PDF)

■ AUTHOR INFORMATION

Corresponding Author

Rui Sun – Department of Chemistry, The University of Hawai'i at Manoa, Honolulu, Hawaii 96822, United States;
orcid.org/0000-0003-0638-1353; Email: ruisun@hawaii.edu

Authors

Kazuumi Fujioka – Department of Chemistry, The University of Hawai'i at Manoa, Honolulu, Hawaii 96822, United States

Ralf I. Kaiser – Department of Chemistry, The University of Hawai'i at Manoa, Honolulu, Hawaii 96822, United States;
orcid.org/0000-0002-7233-7206

Complete contact information is available at:
<https://pubs.acs.org/doi/10.1021/acs.jpca.2c07624>

Notes

The authors declare no competing financial interest.

■ ACKNOWLEDGMENTS

This research is supported by Air Force Office of Scientific Research under grant number: FA9550-21-1-0377. This manuscript is also supported by the National Science Foundation under Grant No. 2144031. The authors appreciate the information technology service (ITS) from the University of Hawai'i, Manoa, and XSEDE for the computational resources.

■ REFERENCES

- (1) Zhang, Y.; Gao, H.; Joo, Y. H.; Shreeve, J. M. Ionic Liquids as Hypergolic Fuels. *Angewandte Chemie - International Edition* **2011**, *50* (41), 9554–9562.
- (2) Chambreau, S. D.; Koh, C. J.; Popolan-Vaida, D. M.; Gallegos, C. J.; Hooper, J. B.; Bedrov, D.; Vaghjiani, G. L.; Leone, S. R. Flow-Tube Investigations of Hypergolic Reactions of a Dicyanamide Ionic Liquid Via Tunable Vacuum Ultraviolet Aerosol Mass Spectrometry. *J. Phys. Chem. A* **2016**, *120* (41), 8011–8023.
- (3) Reddy, G.; Song, J.; Mecchi, M. S.; Johnson, M. S. Genotoxicity Assessment of Two Hypergolic Energetic Propellant Compounds. *Mutation Research/Genetic Toxicology and Environmental Mutagenesis* **2010**, *700* (1), 26–31.
- (4) Wang, S.; Thynell, S. T.; Chowdhury, A. Experimental Study on Hypergolic Interaction between N,N,N',N' -Tetramethylethylenediamine and Nitric Acid. *Energy Fuels* **2010**, *24* (10), 5320–5330.
- (5) Katritzky, A. R.; Rogers, J. W.; Witek, R. M.; Vakulenko, A. V.; Mohapatra, P. P.; Steel, P. J.; Damavarapu, R. Synthesis and Characterization of Blowing Agents and Hypergolics. *Journal of Energetic Materials* **2007**, *25* (2), 79–109.
- (6) Rothgery, E. F. Hydrazine and Its Derivatives. In *Kirk-Othmer Encyclopedia of Chemical Technology*; John Wiley & Sons, 2004. DOI: 10.1002/0471238961.0825041819030809.a01.pub2.
- (7) Troyan, J. E. Properties, Production, and Uses of Hydrazine. *Ind. Eng. Chem.* **1953**, *45* (12), 2608–2612.
- (8) Cardulla, F. Hydrazine. *J. Chem. Educ.* **1983**, *60* (6), 505.
- (9) Malm, J. *Inclusion of Substances of Very High Concern in the Candidate List for Eventual Inclusion in Annex XIV*; European Chemicals Agency, 2013.
- (10) Broadley, J.; Robertson, J. Structure of Dinitrogen Tetroxide. *Nature* **1949**, *164* (4178), 915.
- (11) Schneider, S.; Hawkins, T.; Rosander, M.; Vaghjiani, G.; Chambreau, S.; Drake, G. Ionic Liquids as Hypergolic Fuels. *Energy Fuels* **2008**, *22* (4), 2871–2872.
- (12) Zhang, Q.; Shreeve, J. M. Energetic Ionic Liquids as Explosives and Propellant Fuels: A New Journey of Ionic Liquid Chemistry. *Chem. Rev.* **2014**, *114* (20), 10527–10574.
- (13) Schneider, S.; Hawkins, T.; Rosander, M.; Mills, J.; Vaghjiani, G.; Chambreau, S. Liquid Azide Salts and Their Reactions with Common Oxidizers IRFNA and N_2O_4 . *Inorg. Chem.* **2008**, *47* (13), 6082–6089.
- (14) Xue, H.; Gao, Y.; Twamley, B.; Shreeve, J. M. Energetic Azolium Azolate Salts. *Inorg. Chem.* **2005**, *44* (14), 5068–5072.
- (15) Zeng, Z.; Twamley, B.; Shreeve, J. M. Structure and Properties of Substituted Imidazolium, Triazolium, and Tetrazolium Poly(1,2,4-Triazolyl) Borate Salts. *Organometallics* **2007**, *26* (7), 1782–1787.
- (16) Brotton, S. J.; Kaiser, R. I. Controlled Chemistry via Contactless Manipulation and Merging of Droplets in an Acoustic Levitator. *Anal. Chem.* **2020**, *92* (12), 8371–8377.

- (17) Vogelhuber, K. M.; Booth, R. S.; Annesley, C. J. Theoretical Investigation of the Reactivity of Sodium Dicyanamide with Nitric Acid. *J. Phys. Chem. A* **2018**, *122* (8), 1954–1959.
- (18) Sun, R.; Siebert, M. R.; Xu, L.; Chambreau, S. D.; Vaghjiani, G. L.; Lischka, H.; Liu, J.; Hase, W. L. Direct Dynamics Simulation of the Activation and Dissociation of 1,5-Dinitrobiuret (HDNB). *J. Phys. Chem. A* **2014**, *118* (12), 2228–2236.
- (19) Liu, J.; Zhou, W.; Chambreau, S. D.; Vaghjiani, G. L. Molecular Dynamics Simulations and Product Vibrational Spectral Analysis for the Reactions of NO₂ with 1-Ethyl-3-Methylimidazolium Dicyanamide (EMIM+DCA⁻), 1-Butyl-3-Methylimidazolium Dicyanamide (BMIM+DCA⁻), and 1-Allyl-3-Methylimidazolium Dicyanamide (AM. *J. Phys. Chem. B* **2020**, *124* (21), 4303–4325.
- (20) Liu, J.; Zhou, W.; Chambreau, S. D.; Vaghjiani, G. L. Computational Study of the Reaction of 1-Methyl-4-Amino-1,2,4-Triazolium Dicyanamide with NO₂: From Reaction Dynamics to Potential Surfaces, Kinetics and Spectroscopy. *J. Phys. Chem. B* **2019**, *123* (13), 2956–2970.
- (21) Zhou, W.; Liu, J.; Chambreau, S. D.; Vaghjiani, G. L. Molecular Dynamics Simulations, Reaction Pathway and Mechanism Dissection, and Kinetics Modeling of the Nitric Acid Oxidation of Dicyanamide and Dicyanoborohydride Anions. *J. Phys. Chem. B* **2020**, *124* (49), 11175–11188.
- (22) Mikosch, J.; Zhang, J.; Trippel, S.; Eichhorn, C.; Otto, R.; Sun, R.; De Jong, W. A.; Weidemüller, M.; Hase, W. L.; Wester, R. Indirect Dynamics in a Highly Exoergic Substitution Reaction. *J. Am. Chem. Soc.* **2013**, *135* (11), 4250–4259.
- (23) Sun, R.; Xie, J.; Zhang, J.; Hase, W. L. The F+CH₃I → FCH₃+I-Entrance Channel Potential Energy Surface Comparison of Electronic Structure Methods. *Int. J. Mass Spectrom.* **2015**, *377* (1), 222–227.
- (24) Turner, A. M.; Luo, Y.; Marks, J. H.; Sun, R.; Lechner, J. T.; Klapötke, T. M.; Kaiser, R. I. Exploring the Photochemistry of Solid 1,1-Diamino-2,2-Dinitroethylene (FOX-7) Spanning Simple Bond Ruptures, Nitro-to-Nitrite Isomerization, and Nonadiabatic Dynamics. *J. Phys. Chem. A* **2022**, *126* (29), 4747–4761.
- (25) Luo, Y.; Kang, C.; Kaiser, R. I.; Sun, R. The Potential Energy Profile of the Decomposition of 1,1-Diamino-2,2-Dinitroethylene (FOX-7) in Gas Phase. *Phys. Chem. Chem. Phys.* **2022**, *24*, 26836.
- (26) Mikosch, J.; Trippel, S.; Eichhorn, C.; Otto, R.; Lourderaj, U.; Zhang, J. X.; Hase, W. L.; Weidemüller, M.; Wester, R. Imaging Nucleophilic Substitution Dynamics. *Science* (1979) **2008**, *319* (5860), 183–186.
- (27) Xie, J.; Hase, W. L. Rethinking the SN₂ Reaction. *Science* **2016**, *352* (6281), 32–33.
- (28) Zhang, Y.; Shreeve, J. M. Dicyanoborate-Based Ionic Liquids as Hypergolic Fluids. *Angewandte Chemie - International Edition* **2011**, *50* (4), 935–937.
- (29) OEIS Foundation Inc. *On-Line Encyclopedia of Integer Sequences*. <https://oeis.org>.
- (30) McKay, B. D.; Yirik, M. A.; Steinbeck, C. Surge: A Fast Open-Source Chemical Graph Generator. *J. Cheminform* **2022**, *14* (1), 24.
- (31) Valiev, M.; Bylaska, E. J.; Govind, N.; Kowalski, K.; Straatsma, T. P.; Van Dam, H. J. J.; Wang, D.; Nieplocha, J.; Apra, E.; Windus, T. L.; De Jong, W. A. NWChem: A Comprehensive and Scalable Open-Source Solution for Large Scale Molecular Simulations. *Comput. Phys. Commun.* **2010**, *181* (9), 1477–1489.
- (32) Lee, C.; Yang, W.; Parr, R. G. Development of the Colle-Salvetti Correlation-Energy Formula into a Functional of the Electron Density. *Phys. Rev. B* **1988**, *37* (2), 785–789.
- (33) Francl, M. M.; Pietro, W. J.; Hehre, W. J.; Binkley, J. S.; Gordon, M. S.; DeFrees, D. J.; Pople, J. A. Self-Consistent Molecular Orbital Methods. XXIII. A Polarization-Type Basis Set for Second-Row Elements. *J. Chem. Phys.* **1982**, *77* (7), 3654–3665.
- (34) Henkelman, G.; Uberuaga, B. P.; Jónsson, H. A Climbing Image Nudged Elastic Band Method for Finding Saddle Points and Minimum Energy Paths. *J. Chem. Phys.* **2000**, *113* (22), 9901–9904.
- (35) Fukui, K. Formulation of the Reaction Coordinate. *J. Phys. Chem.* **1970**, *74* (23), 4161–4163.
- (36) Gonzalez, C.; Schlegel, H. B. An Improved Algorithm for Reaction Path Following. *J. Chem. Phys.* **1989**, *90* (4), 2154–2161.
- (37) Lourderaj, U.; Sun, R.; Kohale, S. C.; Barnes, G. L.; De Jong, W. A.; Windus, T. L.; Hase, W. L. The VENUS/NWChem Software Package. Tight Coupling between Chemical Dynamics Simulations and Electronic Structure Theory. *Comput. Phys. Commun.* **2014**, *185* (3), 1074–1080.
- (38) Liu, J.; Zhou, W.; Chambreau, S. D.; Vaghjiani, G. L. Molecular Dynamics Simulations and Product Vibrational Spectral Analysis for the Reactions of NO₂ with 1-Ethyl-3-Methylimidazolium Dicyanamide (EMIM+DCA⁻), 1-Butyl-3-Methylimidazolium Dicyanamide (BMIM+DCA⁻), and 1-Allyl-3-Methylimidazolium Dicyanamide (AMIM+DCA⁻). *J. Phys. Chem. B* **2020**, *124* (21), 4303–4325.
- (39) Zhou, W.; Liu, J.; Chambreau, S. D.; Vaghjiani, G. L. Molecular Dynamics Simulations, Reaction Pathway and Mechanism Dissection, and Kinetics Modeling of the Nitric Acid Oxidation of Dicyanamide and Dicyanoborohydride Anions. *J. Phys. Chem. B* **2020**, *124* (49), 11175–11188.
- (40) Thomas, A. E.; Chambreau, S. D.; Redeker, N. D.; Esparza, A. A.; Shafirovich, E.; Ribbeck, T.; Sprenger, J. A. P.; Finze, M.; Vaghjiani, G. L. Thermal Decomposition and Hypergolic Reaction of a Dicyanoborohydride Ionic Liquid. *J. Phys. Chem. A* **2020**, *124* (5), 864–874.
- (41) Nichols, C. M.; Wang, Z.-C.; Yang, Z.; Lineberger, W. C.; Bierbaum, V. M. Experimental and Theoretical Studies of the Reactivity and Thermochemistry of Dicyanamide: N(CN)₂. *J. Phys. Chem. A* **2016**, *120* (7), 992–999.
- (42) Liu, X.; Zhang, J.; Yang, L.; Hase, W. L. How a Solvent Molecule Affects Competing Elimination and Substitution Dynamics. Insight into Mechanism Evolution with Increased Solvation. *J. Am. Chem. Soc.* **2018**, *140* (35), 10995–11005.
- (43) Okafor, E. C.; Somarathne, K. D. K. A.; Ratthanana, R.; Hayakawa, A.; Kudo, T.; Kurata, O.; Iki, N.; Tsujimura, T.; Furutani, H.; Kobayashi, H. Control of NO_x and Other Emissions in Micro Gas Turbine Combustors Fuelled with Mixtures of Methane and Ammonia. *Combust. Flame* **2020**, *211*, 406–416.
- (44) Stagni, A.; Cavallotti, C.; Arunthanayothin, S.; Song, Y.; Herbinet, O.; Battin-Leclerc, F.; Faravelli, T. An Experimental, Theoretical and Kinetic-Modeling Study of the Gas-Phase Oxidation of Ammonia. *React. Chem. Eng.* **2020**, *5* (4), 696–711.
- (45) Wang, S.; Wang, Z.; Elbaz, A. M.; Han, X.; He, Y.; Costa, M.; Konnov, A. A.; Roberts, W. L. Experimental Study and Kinetic Analysis of the Laminar Burning Velocity of NH₃/Syngas/Air, NH₃/CO/Air and NH₃/H₂/Air Premixed Flames at Elevated Pressures. *Combust. Flame* **2020**, *221*, 270–287.